Functional fluorescent materials and migration dynamics of neural progenitor cells

Bossert, N.

5

NEURAL PROGENITOR CELLS *in vitro* MIGRATION AND BEHAVIOUR

Neural progenitor cells are in the focus of attention for treatment of neurodegenerative diseases and injuries of the central nervous system. As these cells need to migrate to the affected areas upon injection or recruitment, for successful treatments it is crucial to gain more understanding about their migratory dynamics and behaviour. In this chapter, we establish several minimalistic in vitro systems to analyse neural progenitor cells dynamics within a controlled environment and present preliminary results. On the statistical level, we observe that the cells move in a persistent random motion independent of the environment. On the case-by-case level, we observe recurrent behavioral patterns like frequent turning of direction or competing for space that results from the interaction with the environment and neighboring cells.

5.1. INTRODUCTION

Cell migration plays a pivotal role in a myriad of physiological processes, such as immune response, neurogenesis, tissue remodelling, or metastasis. In the case of brain-related disorders, migratory defects can contribute to neurological diseases like epilepsy or mental retardation [1]. Thus, uncovering the principles of cellular dynamics and interactions with neighbouring cells is crucial for our understanding of neurological disease development and their treatments. The motility of a cell is governed by a complex interplay between the cytoskeletal machinery, substrate adhesion units, and environmental sensing. While migrating *in vivo*, cells encounter multiple challenges, like physical constrictions or other cells. Deconstructing this complexity and analysing cellular dynamics and social behaviour *in vitro*, gives valuable insights and enhances our understanding of these processes [2].

One such reductionist approach uses the importance of extracellular matrix (ECM) proteins and mimics the variety of geometries *in vivo* by creating defined protein patterns on 2D substrates *in vitro*. This so called micropatterning spatially controls the adhesive regions, and thus cell attachment, and enables highly reproducible experiments for cell adhesion and migration studies. Studies using this method uncovered interesting findings in cell biology by linking the influence of ECM patterns to cell orientation, directional guidance, and differentiation [3–5]. Further, they are applied for tissue engineering and drug screening [6, 7]. Several techniques were developed to produce these microscopic ECM patterns on substrates, such as micro-contact printing (μCP) [8] and micro plasma-initiated pattern (μPIP) [9] and are employed in this chapter to produce varying geometries.

Despite the complexity of cell migration, the essence of their dynamics over long distances (>> cell body), can be captured by relatively simple mathematical equations of motion [10]. To describe individual cell migration in 2D, the most common model is the persistent random walk (PRW) model that is based on Brownian motion [11]. This model describes that on short times scales, cells display directional persistence, demonstrating a correlation of subsequent steps and ultimately meaning that cells are likely to continue walking in the direction of their previous step. On longer times scales however, in the absence of directional cues, cells display a completely random motion, corresponding to a random walk (RW) model [10]. These modes of migration can be extracted by calculating the averaged explored area over time (i.e., mean squared displacement, MSD) and fitting the models to the acquired data. This approach yields descriptive parameters like persistence time, velocities, and diffusion constant, giving insights into the overall dynamics of cells (for formulas, see section Materials and Methods 5.3).

As described in the introduction in chapter 1, neural progenitor cells (NPCs) are highly motile cells. Due to the increasing motivation to employ these cells for therapeutic purposes, it is crucial to gain more understanding about the basic mechanisms of NPC migration and behaviour. In this chapter, minimalistic systems are established to facilitate research of NPC dynamics. Next to the comparison of NPC migration on two-dimensional substrates that were uniformly coated with different ECM proteins, also micropatterning of diverse geometries is used here to constrict the motion area of NPCs and observe their response.

The dynamics of the cells are analysed by global statistics and further conclusions are

gathered by case-by-case observation. NPCs with fluorescent reporters for cytoskeleton and nuclei (for details see chapter 4) are also employed to facilitate the tracking and observational analysis. Finally, a short look is taken into a further development of the minimalistic systems to the 3D, by establishing microchannels and adding constrictions that mimic the environmental confinement NPCs experience *in vivo*.

5.2. RESULTS AND DISCUSSION

5.2.1. NPCS MIGRATION ON DIFFERENT ECM PROTEINS

In the central nervous system (CNS), various extracellular membrane (ECM) proteins are present. Their role is to structurally and biochemically support the embedded cells and provide attachment sites for migrating NPCs. Fibronectin and laminin are two prominent ECM proteins that are commonly used in *in vitro* cell culture. Here, we compared the basic migratory behaviour of NPCs on a uniform distribution of these two proteins on 2D substrates. Using fluorescence confocal microscopy, time-lapse data was collected with a frame rate of one image every 10 min for a period of 20 h.

To gain insight into the overall behaviour of NPCs, cell trajectories were gathered by tracking fluorescently labelled nuclei (for details see Materials and Methods 5.3). Cells were tracked until they divided and new tracks were started with individual daughter cells. Due to the high proliferation rate of these NPCs, the short time between two divisions lead to relatively short single trajectories. To extend these, a proliferation inhibitor was tested (i.e., RO3306 (SML0569, Sigma-Aldrich). However, this led to dedifferentiation of the cells making this option not feasible (data not shown). To acquire relevant data, trajectory lengths below 30 steps (= 5 h) were excluded from the analysis. The collected trajectories are displayed in Figure 5.1 a, with a uniform distribution of collected trajectory lengths.

Cell trajectory plots (Figure 5.1 b) display a qualitative analysis of the trajectory lengths and travel direction. On both substrates, NPCs move in all directions with a maximum radius of 100 μm. The polar plots of angle distributions (Figure 5.1 c) show a primarily even distribution of cell migration in all directions. As no chemical gradient was employed, this was the expected behaviour as cells normally do not exhibit a preference to any direction without a guiding chemical attractant or repellent.

Statistical analysis of tracking data can give more information about the migration behaviour of cells. Here, the mean squared displacement (MSD) over all trajectories was calculated and plotted over lag time (Figure 5.2 a, b). Fitting the power-law for lag times < 50 min on laminin and fibronectin, resulted in an adequate fit from which average velocities (v_0) and persistence times (τ) were extracted (insets in Figure 5.2 a, b).

The MSD fits on both substrates show that cells exhibit partly directed movement on short time scales (< 50 min), then randomness starts to dominate until the movement results in completely random motion on long time scales (> 100 min). This accurately resembles the PRW model, concluding that although on shorter time scales cells seem to move towards a particular direction, on longer time scales they just randomly explore their environment.

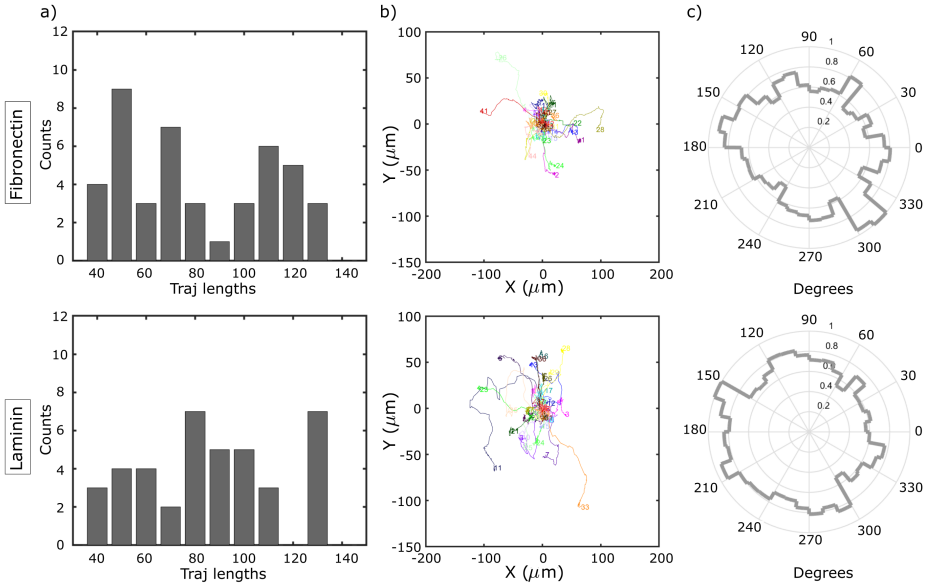

Figure 5.1: Trajectory analysis on ECM proteins. Distribution of trajectory lengths (a) displays the collected and evaluated trajectories on fibronectin and laminin. Cell trajectories plotted centred (b) and angle histogram plots (c) shows directionality of NPC migration on fibronectin and laminin into all directions.

The directional persistence (τ) time of cells characterizes the average time a cell exhibits between significant changes of direction [12]. NPCs observed here had a slightly higher persistence time on fibronectin with 48.7±7.6 min than on laminin with 43.6±2.7 min. The linear fit of the RW model yielded the diffusion constant (D_{eff}) values for cell motion on lag times over 80 min (Figure 5.2 b). Interestingly, the diffusion constants are considerably lower on fibronectin with 0.39±0.03 μm^2/min than on laminin with 1.51±0.06 μm^2/min. Likewise, the approximated average velocity (v_0) for fibronectin with 0.13±0.01 μm/min is almost half of the value on laminin with 0.27±0.01 μm/min (Figure 5.2 a).

Further, instantaneous velocity was calculated, and their respective frequencies were plotted (Figure 5.2 c). The average instantaneous velocity (v) on fibronectin (0.177±0.006 μm/min) was much lower than on laminin, however with a narrow distribution around this value. On laminin, the velocity is almost double with 0.304±0.009 μm/min, but the value distribution is slightly broader here. Comparing the average velocity approximated via the MSD fit (Figure 5.2 a, LN = 0.27±0.01 μm/min, FN = 0.13±0.01 μm/min) with the measured average velocity (Figure 5.2 c), gives a good indication of the accuracy of the fit and supports our results.

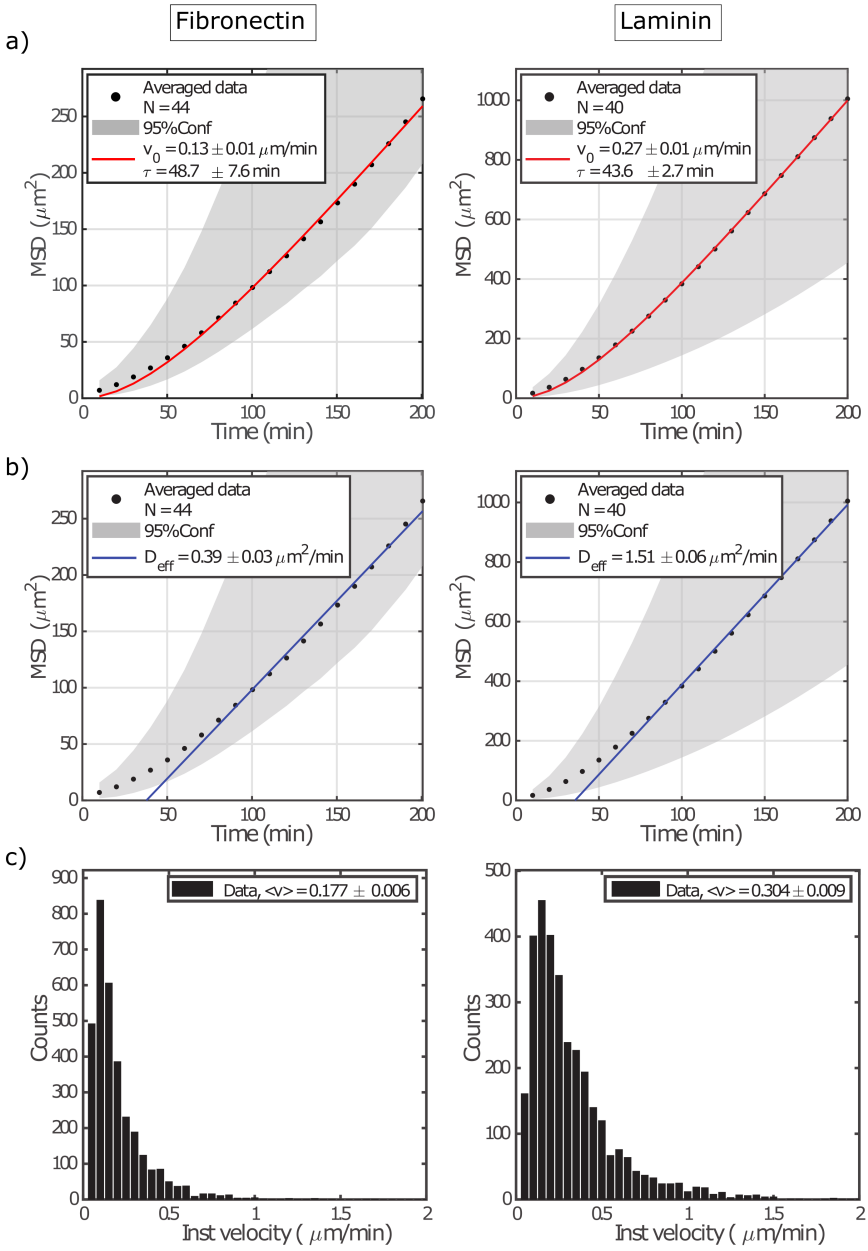

Figure 5.2: NPCs migration on ECM proteins. Mean-squared displacement (MSD) plots of NPC trajectories on fibronectin and laminin with power-law fitted as function of time (a) and linear fit (b) to extract the diffusion constant. Grey area represents the 95% confidence interval of the average of MSDs of all individual trajectories. Frequency distribution of instantaneous velocities and average values for fibronectin and laminin (c).

The explanation for the lower speed values on fibronectin might be explained by an influence of ECM proteins on cell motion. However, the reason here might also be an experimental error in the fibronectin coating. To firmly confirm the cause of the observed difference repetition of these experiments is needed. Interestingly, although the diffusion constant and the velocity are lower on fibronectin, the persistence time is comparable to laminin. Thus, although the fibronectin coating seems to affect cell attachment and thus the speed that the cells can move with, it does not impact the time during which the NPCs are moving in one direction.

CONCLUSIVE BULLET POINTS

Here the results of the current subchapter are summarized:
• NPC migration on uniform laminin and fibronectin substrates can be described by the PRW model
• On laminin, NPCs moved faster compared to fibronectin, with higher average velocities (LN: 0.304±0.009 μm/min, FB: 0.177±0.006 μm/min) and diffusion coefficients (LN:1.51±0.06 μm^2/min, FB: 0.39±0.03 μm^2/min)
• On fibronectin, the persistence times were slightly higher (48.7±7.6 min) than on laminin (43.6±2.7 min)

5.2.2. MIGRATION ON PATTERNED LINES

NPCs use ECM scaffolds, blood vessels, and glia cells as guiding structures while migrating in the brain [13, 14]. Due to the compact environment, NPCs can be constricted to tube-like spaces during migration. To approach the complex *in vivo* situation in a simplified way, line patterns of ECM proteins can be deposited on a two-dimensional (2D) surface, confining the cells to one dimension. Pluronic F-127 is a chemical that was shown to prevent cell attachment [15] and is often employed to enhance selective adhesions of cells to the applied ECM pattern.

Employing micro-contact printing (μCP), we generated fibronectin lines with deposited Pluronic F-127 in the interspaces. To explore the influence of small geometrical variations on NPC dynamics, we created varying line widths of 10 μm (L 10), 15 μm (L15), 20 μm (L 20), and 25 μm (L25). As expected, NPCs aligned on all lines with a broader expansion on lines with increasing width (Figure 5.3). Notably, the ability of cells to align on topographical patterns is important in various physiological contexts [16, 17], known as contact guidance [18]. This phenomenon was reproduced *in vitro* using different patterning techniques [19].

Occasionally, the μCP method did not result in uniform ECM printing (Figure 5.3 c, arrow), whereby the imperfect lines were mostly missing the pattern in its centrum. Thus, the cells could still align to the edges of the pattern, taking up the full line width (Figure 5.3 c), and were thus considered as successfully aligned. However, patterning of the L15 yielded many lines with only a thin pattern on one side. As a high number of lines was still intact, the data is incorporated into the analysis and consequences of the ineffective pattern are pointed out in the respective results section.

To analyse NPC dynamics on the different lines, fluorescence time lapse microscopy was performed for 22h and images collected every 10 min.

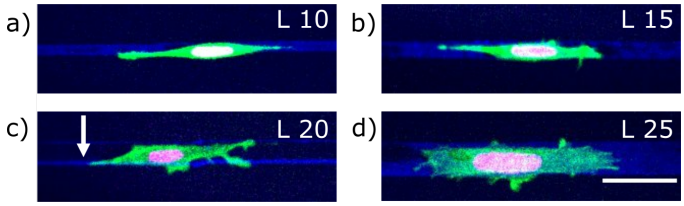

Figure 5.3: NPC alignment on fibronectin lines.NPCs stretch out (both in cell body and nucleus) and align on all patterned lines showing a broader morphology with increasing width (from a to d). Scale is 50 μm.

STATISTICAL ANALYSIS

Statistical analysis of NPC migration was performed on patterned lines as in section 5.2.1 and yielded insights into global behaviour under one-dimensional confinement. As before, trajectory lengths below 30 steps were excluded from the analysis, yielding a uniform distribution of trajectory lengths (Figure 5.4 a). As expected, direction of movement was highly constricted to the x-axis on L10 and shows increasingly more movement into y-direction on wider L25 (Figure 5.4 b). The maximum walked distance in x-direction was 200 μm (Figure 5.4 b) and thus longer than without confinement (section 5.2.1). Angle histograms are illustrating the motion constriction to x-direction and the slight additional range of motion that cells experience on wider lines (Figure 5.4 c).

Global MSD calculations with subsequent PRW and RW fits were applied (as in section 5.2.1) to gather data about the overall NPC dynamics on pattered lines. Both fits accurately followed the calculated data points for all line widths, except for L15. Here, the PRW fit is more linear than exponential at short lag times (Figure 5.5 a, L15), and the RW fit aligns with the data points earlier (Figure 5.5 b, L15) compared to the other line widths (Figure 5.5 b). This alignments suggests a low persistence and mainly random motion on L15, as can also be seen on the calculated persistence time (τ) (Figure 5.5 a, L15, inset) that is about half the value of the persistence times on the other lines.

These result might be explained by the ineffective patterning of L15 as was pointed out above. Additionally, at the start of the experiment, the cells on L15 were present in a slightly higher number (L15 = 55 cells) compared to other lines (L10 = 42 cells, L20 = 50 cells, L25 = 28 cells). These two conditions together probably created obstacles for the NPCs and inhibited movement into one direction for longer times. As NPCs encountered the discontinuity in pattern and/or other cells more frequently on L15 than on other lines, this resulted more often in the interruption of their moving direction, yielding the considerably lower persistence time value.

On lines L10, L20, and L25 the persistence times of motion are fairly similar with 19.7±1.2 min, 25.3±2.7 min, and 20.9±2.8 min, respectively (Figure 5.5 a). However, on L20 the persistence time is the highest with 25.3±2.7 min. Interestingly, also the velocity has the highest value on L20 compared to the other lines (Figure 5.6 c). A hypothesis to explain this result might be that a width of 20 μm provides a good balance between contact guidance and sufficient space for proper cell attachment and movement, thus facilitating faster and more directional migration of NPCs. In comparison to uniform substrates (LN: 43.6±2.7 min, FB: 48.7±7.6 min), the persistence times are considerably lower. This can be due to several reasons. NPCs are here restricted to one dimensional movement which leaves them with a binary decision to go either left or right. The confinement leads to the inevitability of encountering other cells in the way, forcing the NPCs to change their directed motion. In contrast, on the uniform substrates NPCs have all degrees of freedom to move in any direction for longer times.

Another explanation might be rooted in the confinement of the cells, which changes the physical dimensions of the system to nearly 1D and thereby also the associated equations. This influences the values found for both, the persistence time and diffusion constant in the PRW and RW fits, but not the velocities (as this is independent of the dimensionality). Interestingly, the persistence times on lines are about half the values compared to the times on 2D laminin. By adjusting the equations to 1D (for details see Materials and Methods section 5.3), the calculated persistence times would be 39.4±2.4 min, 50.6±5.4 min, and 41.8±2.8 min for L10, L20, and L25, respectively, which are more comparable to the value on 2D laminin with 43.6±2.7 min (section 5.2.1, Figure 5.1). The calculated diffusion coefficients on L10, L15, L20, and on L25 are 0.9±0.01 μm^2/min, 0.98±0.02 μm^2/min, 0.99±0.03 μm^2/min, and 0.90±0.01 μm^2/min, respectively (Figure 5.5 b). Again, finding the highest motion value for L20, like in our previous observations, these results support a facilitation of the NPCs migration on lines of 20 μm width. Notably, the ineffective patterning of L15 and the higher cell number did not influence the inherent motion of NPCs (like it did for the persistence time), as the velocity and the diffusion values do not diverge from the values on other lines.

Figure 5.4 ***(following page)*****: Trajectory analysis on fibronectin lines.** a) Left column, distribution of trajectory lengths displays the collected and evaluated trajectories on L10, L15, L20, and L25 lines. b) Middle column, spatial plots of cell trajectories showing the directionality and range of NPC movement. Note, the X and Y axis differ in scale by about 10-fold. c) Right column, angle histogram plot displaying restricted cell movement to the X plane and increasing movement in the Y plane with wider lines (from L10 to L25).

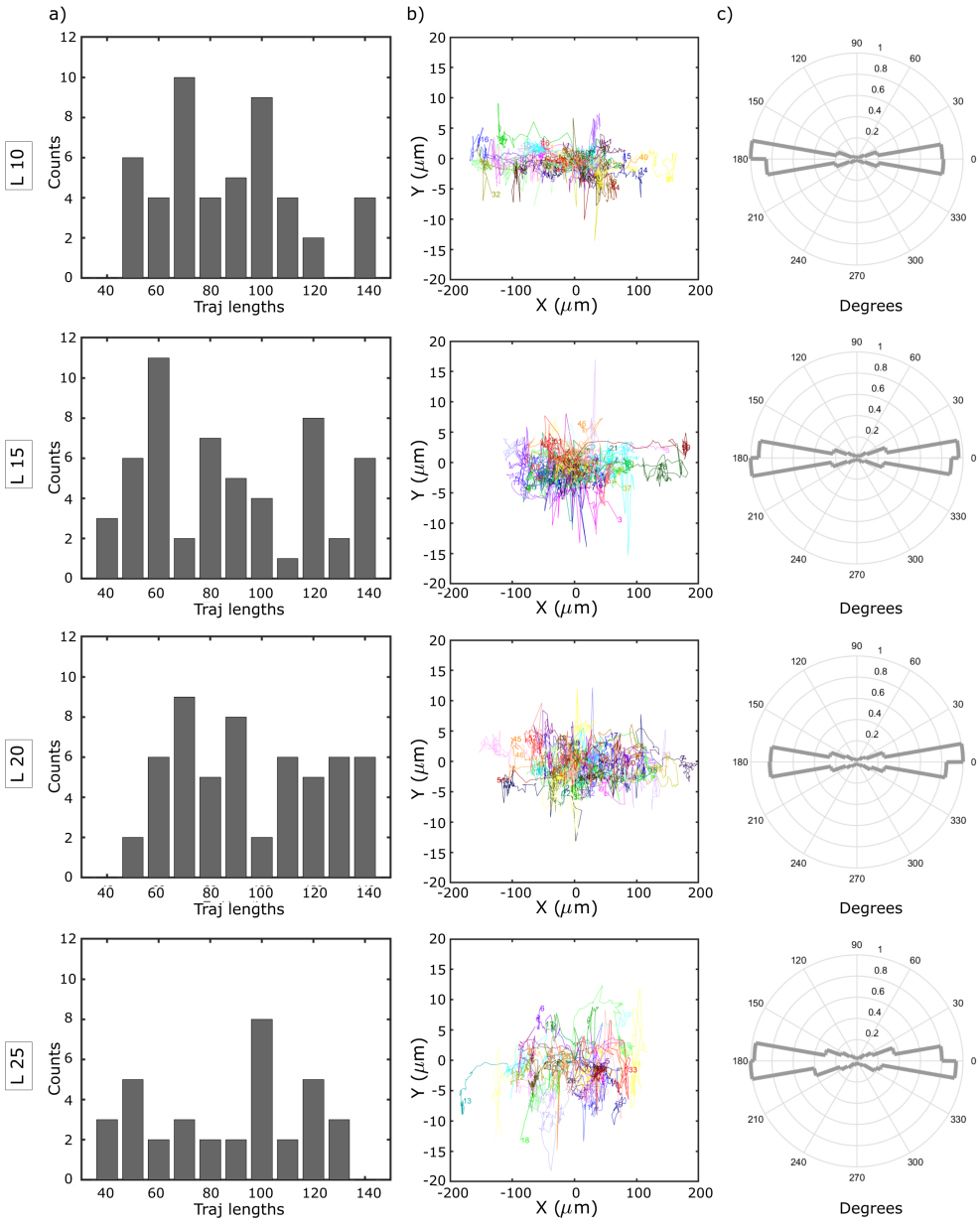
a)
b)
c)
L 10
L 15
L 20
L 25
Counts
Traj lengths
Y (μm)
X (μm)
Degrees

Taking into account the one-dimensionality (1D) of the lines and adjusting the formulas also in this case (for details see Materials and Methods 5.3), leads to diffusion constants of 1.79±0.01 μm^2/min, 1.96±0.04 μm^2/min, 1.98±0.06 μm^2/min, and 1.80±0.02 μm^2/min for L10, L15, L20, and L25, respectively. These results are comparable to uniform laminin with 1.51±0.06 μm^2/min but lie above its value. Thus, the 1D values, collected on lines, are not a perfect half of the 2D value, collected on plain surfaces. This can be explained by the fact that this is a biological system that we observe and not an ideal system, yielding an environment in which the NPCs have still some freedom in movement on the lines and beyond, thus influencing the calculated values.

The velocity values on the lines are similar with 0.284±0.008 μm/min, 0.304±0.009 μm/min, 0.268±0.008 μm/min, and 0.28±0.1 μm/min for L10, L15, L20, and L25, respectively (Figure 5.6. These values lie within the range of published mean velocity values (0.1 - 1 μm/min) that were collected in a World Cell Race with 54 different cell types, performed on printed 4 μm and 12 μm lines [20]. Compared with the tested highly migratory cell types, NPCs correspond to the rather slow-moving cells.

Comparing the velocities on lines to the velocities gathered on plain 2D surfaces (section 5.2.1), the averaged velocity values are comparable to the value on laminin substrate (0.304±0.009 μm/min, Figure 5.2). Coming back to the velocity results on plain fibronectin surface, whereby an experimental error in deposing the protein might have caused the lower value, another point would be interesting to consider here. Assuming, that the motion of uniform fibronectin was indeed slower than on uniform laminin, but the velocity values on fibronectin lines are comparable to the values on uniform laminin, using unidirectional lines might have increased cell velocity. In previous studies it has been shown that contact guidance by topographical cues does enhance the migration velocity compared to migration on a uniform substrate [21]. To make a valid conclusion in this case, additional experiments are needed to exclude experimental errors and additionally generate patterned laminin lines to compare the data comprehensively.

Figure 5.5 *(following page)*: Cell migration of NPCs on fibronectin lines. Mean-squared displacement (MSD) plots of NPC trajectories on L10, L15, L20, and L25 lines. a) Power-law is fitted (red) to the MSDs as a function of time displaying persistence times (τ) and approximated velocities (v_0). b) A linear fit (blue) to the MSDs (middle) to extract the diffusion constant. Grey area represents the 95% confidence interval of the average of MSDs of all individual trajectories.

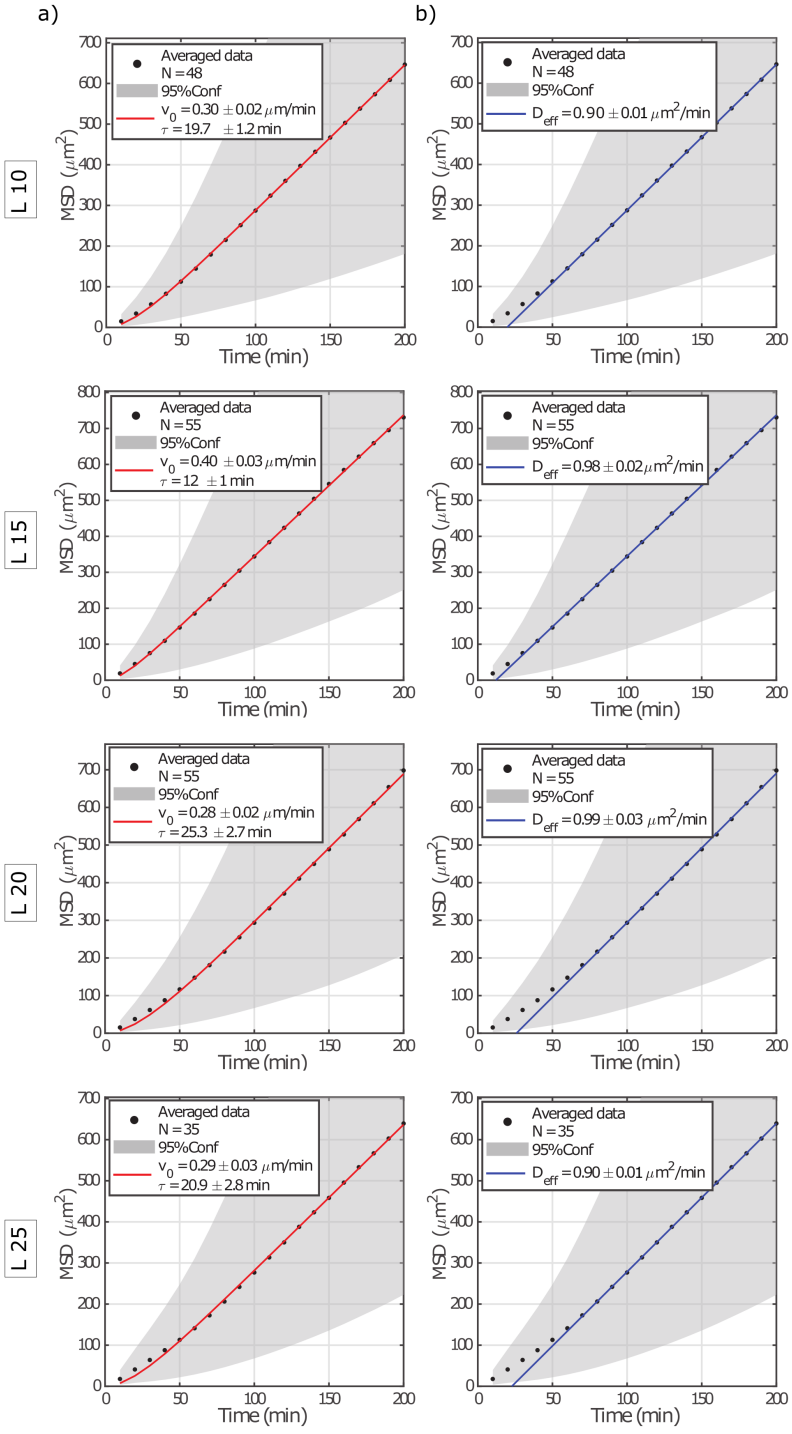
a)
b)
L 10
L 15
L 20
L 25
Averaged data
N = 48
95%Conf
v0 = 0.30 ± 0.02 μm/min
τ = 19.7 ± 1.2 min
Deff = 0.90 ± 0.01 μm²/min
N = 55
v0 = 0.40 ± 0.03 μm/min
τ = 12 ± 1 min
Deff = 0.98 ± 0.02 μm²/min
v0 = 0.28 ± 0.02 μm/min
τ = 25.3 ± 2.7 min
Deff = 0.99 ± 0.03 μm²/min
N = 35
v0 = 0.29 ± 0.03 μm/min
τ = 20.9 ± 2.8 min
Deff = 0.90 ± 0.01 μm²/min
MSD (μm²)
Time (min)

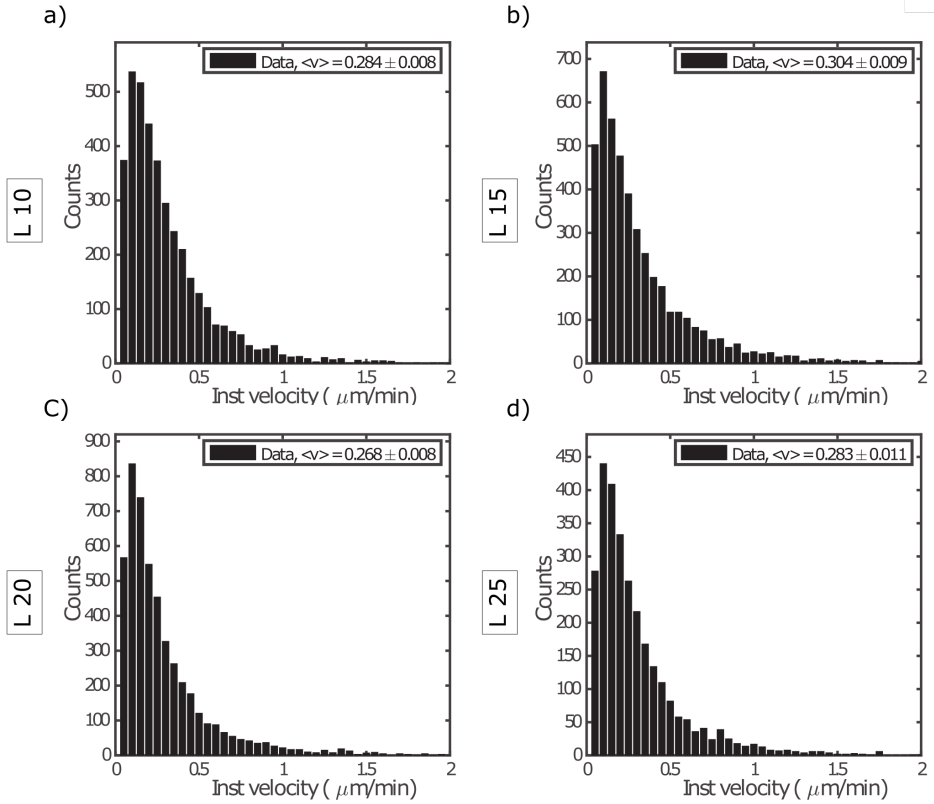

Figure 5.6: Cell migration of NPCs on fibronectin lines. Instantaneous velocity on L10, L15, L20, and L25 lines. The frequency distribution of instantaneous velocities and average values for all line widths.

5

VISUAL OBSERVATIONS

Statistical analysis provides useful information about NPC dynamics. However, as solely nuclei were used for cell tracking and the calculated values are averaged, it cannot capture the details of cell behaviour. By restricting NPC movement to line patterns, additional complexity was introduced to the system, making direct observation of the NPCs movement more necessary. Thus, time-lapse data was also analysed via visual observations whereby repeated behavioural patterns in NPCs were detected. These behaviours were found to occur on all lines, independent of the widths. Thus, only selected representative images are shown and discussed in this subsection.

Cell migration is a multistep action that is initiated by the polarization of the cell body, whereby the front and the rear of the cell become clearly distinguishable. The cell extends actin-based membrane protrusions at its leading edge, called lamellipodia and filopodia, which are a flat and an almost organelle-free region. The process continues with adhesion to substrate near the front edges of these protrusions, then the cell body contracts, and the cell releases the substrate adhesions at its rear end, thus moving the cell body forward (Figure 5.7) [22]. These morphological dynamics were clearly observed

in NPCs on patterned lines, thanks to an actin-GFP -reporter (Figure 5.8 a). Interestingly, NPCs were found to regularly reverse into opposite direction. Each time, cells elongated a new process into the new direction and retracted the pre-existing leading process.

In the representative image sequence, the observed cell changed its direction on the line six times within 630 min (Figure 5.8 a.) NPCs exhibited this behavioural pattern although there was no obvious obstacle like another cell or discontinuation of the line. Consistent with these results, previous observation of SVZ neuroblasts showed that they routinely change direction from a few degrees to complete reversals [23]. A previous study by Martinez-Molina *et al.* (2011) analysed in detail neuroblasts turns and direction changes in brain slices and observed an array of different turning types [24]. They found three different patterns of directional reversals, whereby the reversal in 180 °, as observed in our experiment, was the second most common form. Thus, restricting NPCs to a unilinear pattern can help to specifically research one form of directional reversals that NPCs exhibit naturally *in vivo*.

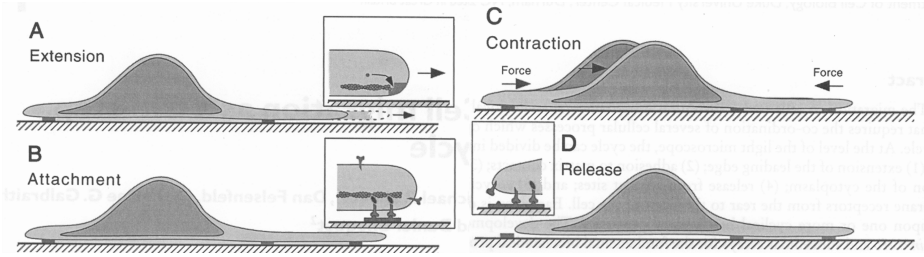

Figure 5.7: Illustration of cell migration steps.a) Extension: Assembly of actin filaments drives protrusion of cell membrane and the extension of the leading edge. b) Attachment: Focal adhesions are formed to attach the new leading edge to the substrate. c) Contraction: The cell contracts, together with Release (d) this results in forward locomotion. d) Release: Focal adhesions at the rear part of the cell are relased. Figure reprinted from Sheetz *et al.* (1999)[25]

.

Exhibiting frequent reversals and thus lacking a long-term directional persistence, these NPCs clearly exhibit “exploratory behaviour” [24, 26]). These observations support the PRW model found in the statistical analysis, showing that on short time scales cells move directionally and on long timescales their movement is random. In accordance with the observed behaviour, migrating neuroblasts in post-stroke striatum were found to spend time exploring their environment and change their direction frequently [13, 27]. This low directional migration was suggested to occur due to an insufficient production of directional cues, associated with adult mammalian’s brain low capacity for regeneration. As in our experiments no chemoattracts are employed, this resembles the observed *in vivo* situation when lacking sufficient directional cues.

Exploring the environment by changing directions and probing it with extending and retracting protrusions is crucial for cells to sample their environment and receive fine-tuned directional information. Additionally, to extending protrusions along patterned lines, NPCs often explored the interspace between the lines (Figure 5.8 b). Due to the non-adhesive substrate (Pluronic F-127) that was used to enforce specific cell attach-

ment to patterned lines, NPCs were clearly not able to adhere at the interspaces resulting in the formation of ruffles in lamellipodia (Figure 5.8 b). Membrane ruffles is a common occurrence which was found to originate when the lamellipodia failed to properly attach to substrate and consequently were retracted towards the cell body, producing a wave-like appearance [28].

At times, NPCs were observed to stretch out until the neighbouring line and "jump" over (Figure 5.9). The distance between the lines was 100 μm, showing the considerable flexibility and reach of these cells. Due to heterogeneity of ECM and microenvironment *in vivo*, cells require the ability to span over non-adhesive gaps. This so called "bridging" is crucial to achieve mechanical stability and integrity of tissue in processes like wound healing, regeneration, and development [29]. Using micropatterned lines, Buskermolen *et al.* (2020) recently analysed myofibroblasts bridging by modifying the line widths and interline spacings. They found that the cells were still able to span lines at 20 μm interspacing but not anymore at 50 μm [30]. However, interline jumps, as observed here, were not reported.

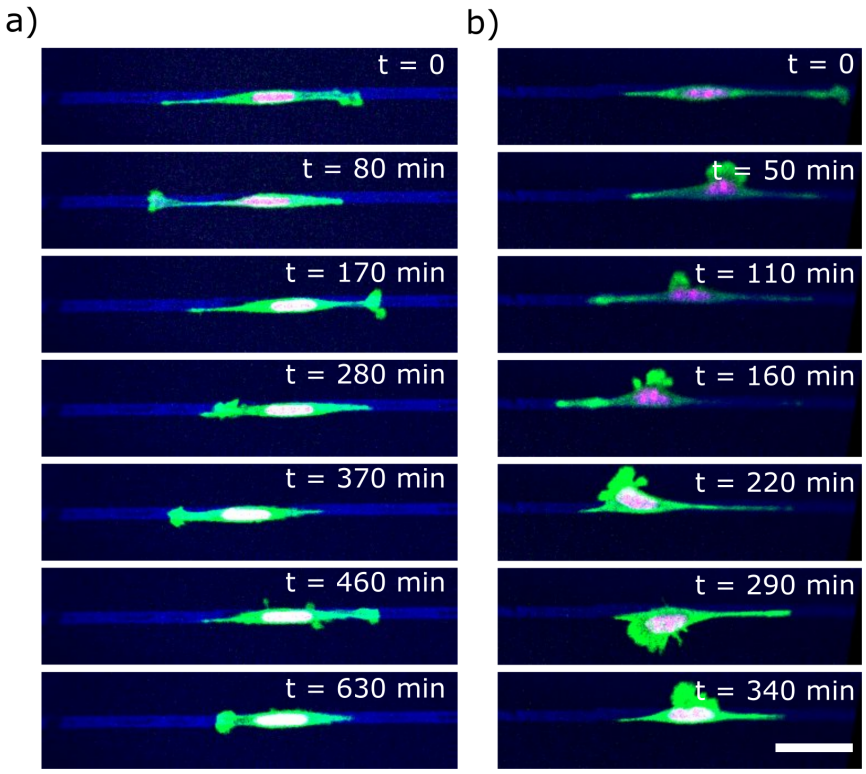

Figure 5.8: Individual NPCs exploring environment. a) Migratory shape of NPC as in Figure 5.7 with polarized cell body is frequently reversing its direction. b) NPC is extending lamellipodia into the line interspace. Scale 50 μm.

Here, it seems like NPCs were able to stretch over the non-adhesive gaps and attach their lamellipodium to another line but did not remain in a bridged state and pulled over to the other side (Figure 5.9). Comparing literature and our data it might be that a bridged state was either not possible at the large distance of 100 μm or it was simply not energy efficient for the NPCs.

Notably, jump events were less frequent on L25, than on the thinner lines. Possibly, on wider lines NPCs were able to stretch out and take up more space thus displaying less motivation to explore. As stated before, cell speed was comparable on all line widths, excluding the possibility that on L25 NPCs were less motile and thus jumped less.

Every cell divided 1 - 2 times throughout the imaging duration of 22 h. When NPCs entered mitosis, they exhibited the typical round shape, and their "anchorage" fibres were clearly oriented along the patterned line (Figure 5.10 a, first image). When cells round up and the cell membrane retracts during mitosis, retraction fibres remain attached to the substrate to ensure cell stability and retention of orientational information. Using micropatterns, researchers found that the orientation of the mitotic spindle is determined by the polarity of the cytoskeletal network and adhesion forces, and consequently modifying micropattern geometry results in different division orientations [31, 32]. Thus, our observation of the NPC division orientation along the lines is comparable with previous studies by exhibiting this conserved mechanism.

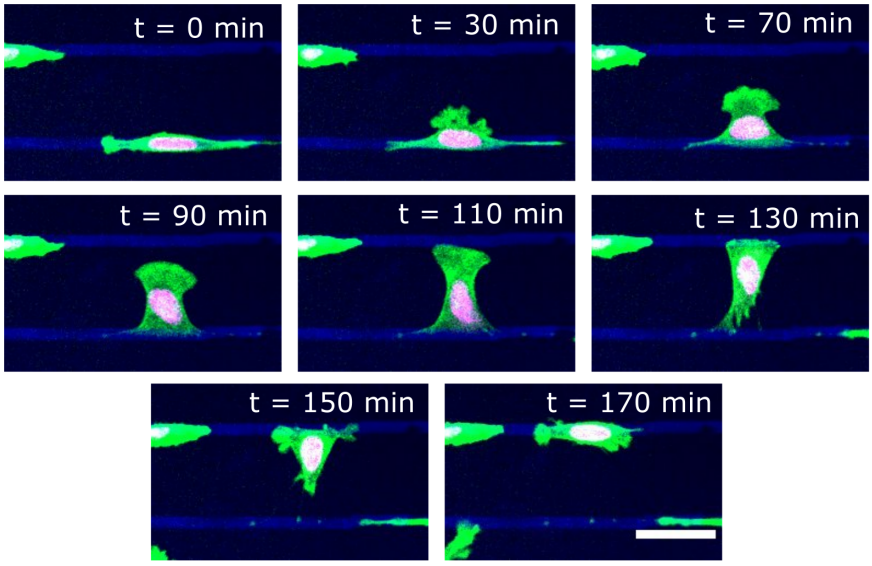

Figure 5.9: NPC jumping between lines. NPC extending over the interspace region between two lines until it reaches the neighboring line and pulls the cell body over. Scale 50 μm.

Interestingly, directly following division, NPCs show directional movement away from each other for up to 50 min after division (i.e., 5 time frames) (Figure 5.10 a). As observed in our experiment, Dix *et al.* (2018) found the same behaviour for RPE1 cells on lines

that, in their shown example (Figure S1 in Dix *et al.* (2018) [33]), migrated away from each other for 90 min after division. This process is crucial for daughter cells to separate from each other after mitosis and re-spread. Using this process to guide cell direction after mitosis might be a valuable asset to control NPC spreading in CNS implants.

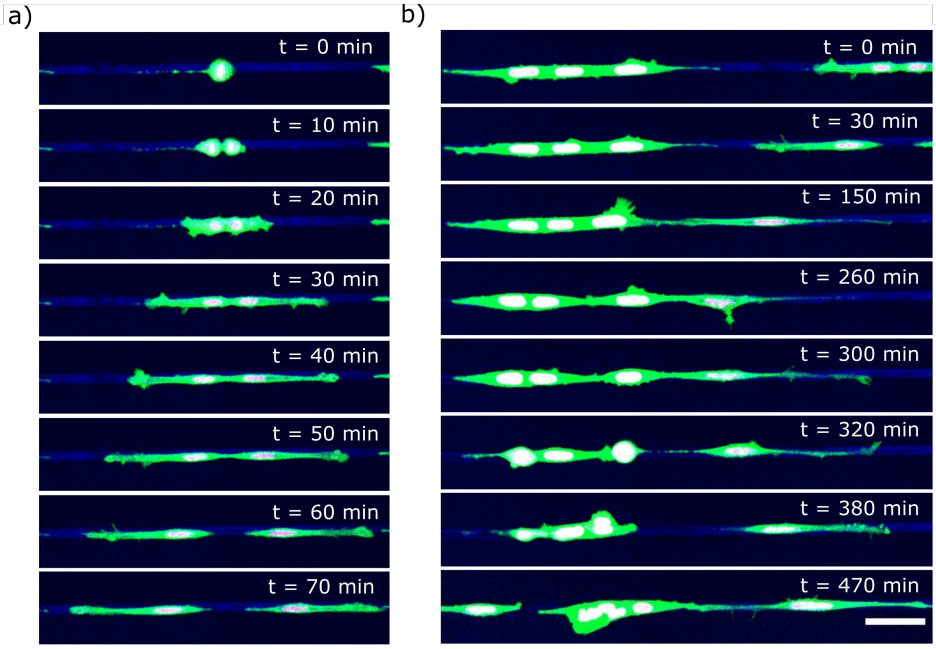

Figure 5.10: NPC mitosis and social behaviour on lines. a) Upon mitosis, daughter cells migrate into opposite direction. b) Upon encountering a cell ensemble, NPC first exhibits contact inhibition of locomotion (t = 380 min) and then reconnects again (t = 470 min). Scale bar 50 μm.

A last striking behavioural pattern was the preference of NPCs for each other's company. Cells often accumulated with 4 - 6 neighbouring cells, although there was enough space available to move away (Figure 5.10 b). However, NPCs did not accumulate all together, but rather found a balance between exploratory single cells and collective assemblies. Notably, these states were often temporary as NPCs kept moving and interacting. A crucial aspect of cell migration *in vivo* is the direct interaction with other cells. Hereby, cells communicate with each other via chemical and physical interactions, and cell-cell contacts play a major role in coordinating their behaviour [34]. Thus, for these NPCs physical contact seems to be particularly important and would be highly interesting to investigate in detail in further experiments.

While migrating *in vivo* or on 2D substrates, cells often collide with other cells. In various publications, micropattern techniques have been used to explore collisions of migrating cells on lines patterns [35, 36]. Hereby, different behavioural patterns have been observed: Upon head-to-head collisions, cells can react with contact inhibition lo-

comotion (CIL), showing repulsive behaviour and moving away from the contacted cell [37]. When a cell walks into the tail end of another cell, contact following of locomotion (CFL) has been observed, whereby the cell starts migrating towards the tail of the neighbouring cell [35].

Analysing our data for these behaviours, we found only rare occasions of CIL. One example of CIL is shown in Figure 5.10 b, whereby one cell (from right) bumps into a cell assembly (on the left) and reverses its movement. Notably, this cell just divided and thus had the momentum of migrating away from its sister cell. This indicates that cells need a certain minimum of directional persistence and speed to exhibit CIL. Thus, the reason for low occurrence of CIL in our experiments, might be that NPCs here do not exhibit high directional persistence and often reserve direction thus not fully colliding into their neighbours. However, to form and test this hypothesis further experiments are required.

Neuroblasts migrating in the rostral migratory stream (for more details, see chapter 1) often move in chains [14], thus making CFL an expected behaviour. However, NPCs were not observed to collide and follow the tail of other cells, which must be due to the lack of real colliding events, as stated above. Notably, walking by or over other cells was another common behaviour NPCs exhibited when neighbouring cells were in their path, showing a rather different behaviour than CIL or CFL.

CONCLUSIVE BULLET POINTS

Here the results of the current subchapter are summarized:

Statistical analysis

• On 2D printed lines, NPCs follow the PRW motion model
• Average velocity values are 0.284±0.008 μm/min, 0.304±0.009 8 μm/min, 0.268±0.0088 μm/min 0.283±0.011 μm/min for L10, L15, L20, and L25, respectively • Persistence times of motion are with 19.7±1.2 min, 25.3±2.7 min, and 20.9±2.8 min for L10, L20, and L25, respectively
• Diffusion coefficients are 0.9±0.01 μm^2/min, 0.98±0.02 μm^2/min, 0.99±0.03 μm^2/min, and 0.90±0.01 μm^2/min for L10, L15, L20, and L25, respectively
• Together, NPCs move slightly faster on L20 lines than on other lines, thus indicating that a width of 20 μm might facilitate cell motion

Observational analysis

• NPCs frequently reverse direction as do neuroblasts *in vivo*
• NPCs show highly explorative behaviour, with short directional persistence thus confirming PRW also by visual observations
• NPCs do not bridge non-adhesive regions, but jump to neighbouring lines
• Upon mitosis, NPCs separate and migrate away from each other
• NPCs stay as single cells and accumulate in small groups
• NPCs hardly show collisions upon locomotion in our experiments, and thus hardly exhibit CIL or CFL behaviour

5.2.3. MORE COMPLEX 2D GEOMETRIES

As stated above, NPCs migrate through a complex ECM network and use blood vessels and astrocytes as guiding scaffolds. These structures intersect and branch, providing a variety of challenges and cues to migrating NPCs. Another crucial aspect of cell migration *in vivo* is the direct interaction with other cells. To approach this higher complexity in a minimalistic way, we created different 2D laminin micropattern geometries using honeycomb and square patterns in a smaller and larger size variation. This allowed to tackle broader geometrical substrate variation, and influence and observe single cell-cell contacts. Length parameters of both patterns until intersections were 50 μm and 150 μm, further referred to as "small" and "big". Big honeycomb and squares were provided with small islands around the intersection to promote cell spreading in these regions and isolate the protrusions. Pattern widths were set to 10 μm, to approach the diameter of blood vessels in murine brains by still accounting the lack of 3D space [38].

To catch the dynamics of NPCs, time lapse of 15 h duration with brightfield images every 1 min were performed. For these experiments, solely analysis by visual observations was employed and a set of behavioural patterns in NPCs was found on these geometries. As the big honeycomb pattern resembles the cerebral vasculature arrangement the most, taking into account the high simplification and placement on 2D substrate, we primarily focused on the analysis of this geometry. Important to note here is that upon analysis it became clear that resulting widths of big honeycomb and squares arms were not 10 μm but below 5 μm. This probably occurred due to technical difficulties of μPIP with this pattern, whereby the plasma was not able to entirely flood through the full width of the arm channels. However, as murine brain capillaries have been measured to have a mean diameter around 4 μm [38], we proceeded our analysis with these patterns.

On all patterns, changes of cell shapes were observed that were imposed by the NPCs spreading on the 2D confined environment. This behaviour is consistent with literature were cells seeded on patterned adhesive proteins were shown to spread out and adapt to shape and size of the pattern [39].

On the big honeycomb patterns, on rare occasions NPCs have been found to stretch out along the arm (Figure 5.11 a). However, as intended by placing islands at intersections, NPCs preferred to spread at the intersections, extending their protrusions to all three directions (Figure 5.11 b). Interestingly, in these states several NPCs were found to stay in a stretched out state for a long time without changing their morphology. In the shown example, NPCs extended on the line remained for 527 min, and on the intersection for 300 min. On small squares and honeycombs, NPCs often spread over 2-3 pattern units, trying to take up more space. Here, cells were more mobile as compared to the big patterns.

As established in section 5.2.2, explorative motion is innate to NPCs. Likewise, on these more complex geometries, NPCs were found to explore their surroundings. However, on these patterns the cells were mostly stationary and explorative dynamics were primarily performed via lamellipodia and filopodia extensions. Figure 5.11 c exemplifies this behaviour, showing a cell centred at the intersection of the honeycomb and extending its lamellipodia into all three directions. Nam *et al.* (2007) found that stationary cells *in vivo* exhibited longer and more processes. Together with our observations, this sug-

gests that when the cell body remains immobile, the cell uses its processes to explore the area and collect directional cues.

Migration of NPCs was only observed right after cell division (Figure 5.11 d), whereby the daughter cells walked for a short distance away from each other (as already discussed in section 5.2.2). An intriguing question would be where the lines is between NPCs showing migratory behaviour and NPCs preferring to align on pattern and remain rather stationary? Most cell types migrate on unidirectional lines [20] and align and stretch out on other geometrical patterns [39]. Thus, it would be interesting to create geometrical variations to tackle this question.

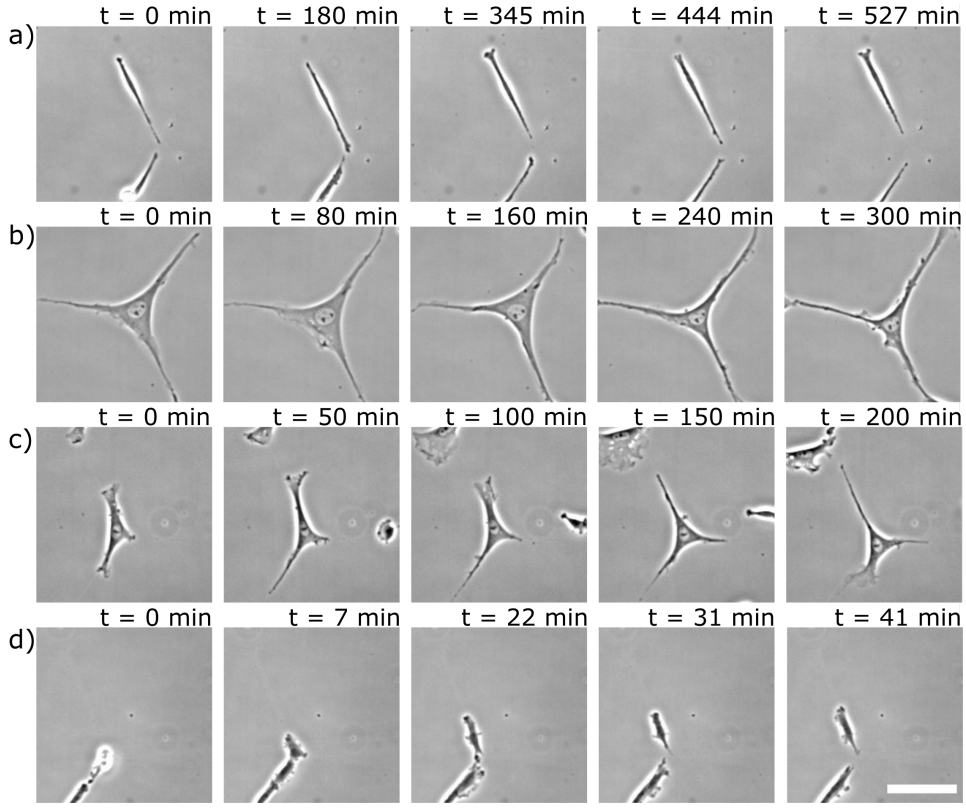

Figure 5.11: NPC distribution and pattern formation after 15 h. NPCs align on the small honeycomb by stretching between two intersections (a), whereas on the big honeycomb (b), small squares (c), and big squares (d), NPCs mainly place their bodies at the intersections. This repetitive behaviour results in a pattern formation. Scale bar is 100 μm.

The employed geometries and used cell seeding numbers allowed for regular cell-cell interactions. Interestingly, NPCs were often observed to tackle each other with their protrusions, appearing to also push and fight for space (Figure 5.12). Figure 5.12 a shows how one NPCs occupies the intersection and interacts via its protrusion with a neigh-

bouring cell. First, the NPC is extending the protrusion, forcing back the protrusion of the neighbouring cell, but then gives in to the extension of the neighbouring cell.

Another example for space competition shows how three NPCs extend their protrusions towards one intersection, whereby one NPC coming from above moves faster towards it and takes the space over by spreading its cell body over it (Figure 5.12 b). Figure 5.12 c exemplifies how three NPCs occupy one honeycomb intersection until one NPC is defeated. Upon giving up the space it allowed the other two cells to spread out more. The last scenario shows a cell division on the intersection resulting in two daughter cells competing for the space (Figure 5.12 d).

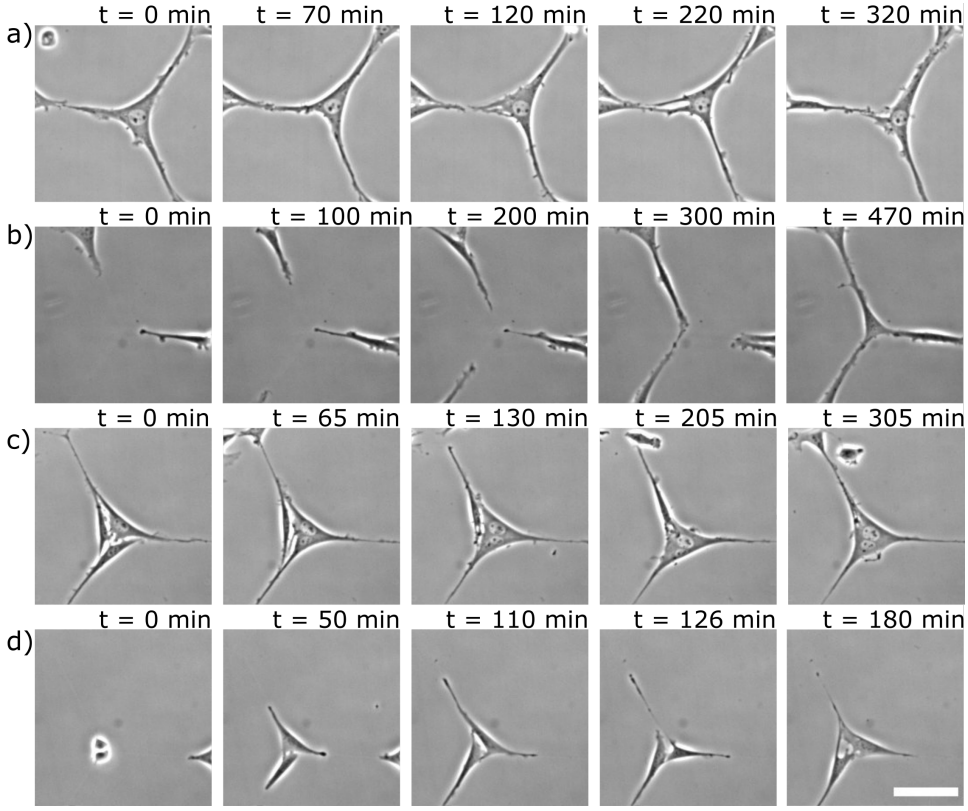

Figure 5.12: NPC competition for space on honeycomb intersections. a) NPC is stretched out at the intersection and is using its extension to push against a cell invading from the left side. b) Three NPCs are competing for the space at one intersection, whereby the left cell loses and retracts in the last two frames. c) From all three sides, NPCs are moving towards one intersection, whereby the cell coming from above manages to place its body and stretch out slightly in the last frame. d) Upon mitosis, daughter cells are stretching out and competing for the space at the intersection. Scale bar is 50 μm.

Except for literature analysing collisions upon locomotion (see section 5.2.2), no publications have been found researching the topic of competition for space, especially on an individual cell level. Thus, this observations are highly interesting. Using our set-up would be ideal in creating a framework to research this competitive behaviour in detail and contributing to our understanding of NPC migratory behaviour and distribution *in vivo*.

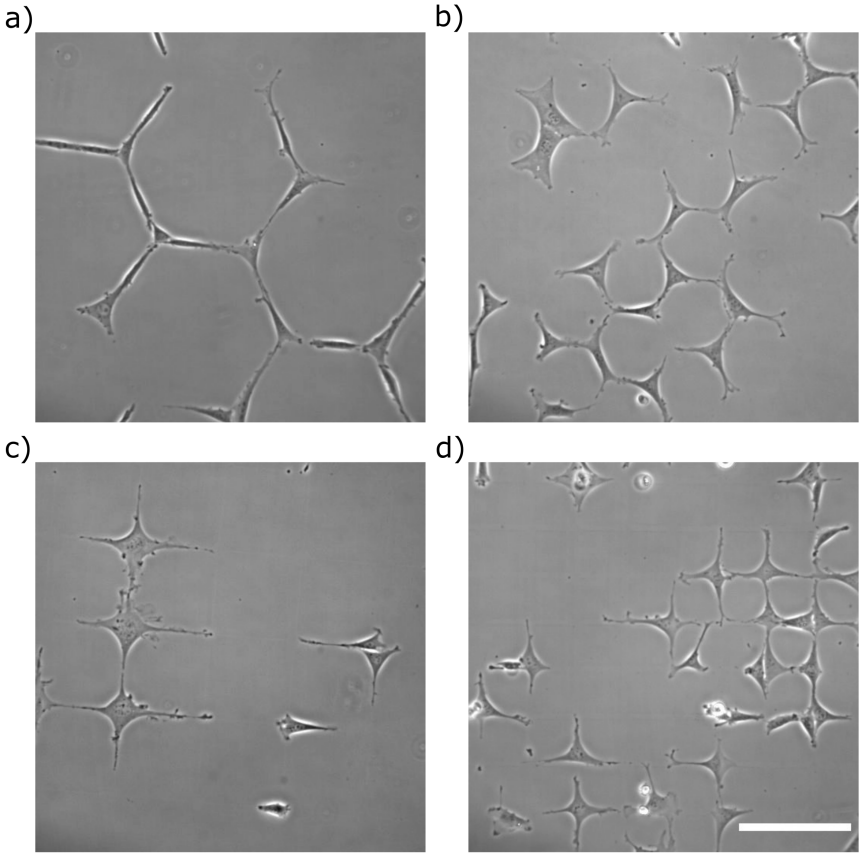

Figure 5.13: NPC distribution and pattern formation after 15 h. NPCs align on the small honeycomb by stretching between two intersections (a), whereas on the big honeycomb (b), small squares (c), and big squares (d), NPCs mainly place their bodies at the intersections. This repetitive behaviour results in a pattern formation. Scale bar is 100 μm.

All described behaviours together result in a nearly homogeneous spreading of NPCs on the patterns (Figure 5.13). The ongoing exploration of the environment, the alignment of cell morphology to the pattern, and the competition for bigger space all lead to a "network" of NPCs on the patterned geometries. Once the space is distributed, the cells keep their network for longer time scales and adjust only when they are dividing and producing more progeny to share the space with.

On small honeycomb pattern (Figure 5.13 b), NPC often stretch in between two intersection, connecting their two arms on side with two arms of the neighbouring cell. On the big honeycomb, cells either stretch out on the intersections or align in between them (Figure 5.13 a). On squares, big and small, NPCs prefer to place their body on the intersections and spread their protrusions in all four directions (Figure 5.13 c, d).

CONCLUSIVE BULLET POINTS

Here the results of the current subchapter are summarized:

• By using more complex geometries, we observed additional behaviours to those found on patterned lines (section 5.2.2)
• NPCs are rarely migrating and are rather stationary with highly dynamic protrusions
• When individual NPCs elongate or spread out taking up more space, they often keep their shape including their protrusions static (until mitosis)
• NPCs compete for space on intersections
• With time, NPCs distribute the space nearly evenly, producing "networks" on the patterns

5.2.4. MICROCHANNELS AND CONFINEMENT

In vivo, cells migrate through dense three-dimensional (3D) environment passing through different barriers imposed by the microstructural extracellular matrix (ECM) and other cells. Adherence to their surrounding in all directions and the possibility to use all sites to push themselves forward, influences the migratory dynamics of cells. Thus, as a next step in in attempting a more detailed understanding of NPC migration behaviour *in vivo*, a minimal 3D-environment system is introduced below. Here, only first experiments were performed and are shortly discussed, as for a full analysis more data is required.

By using PDMS moulded microchannels placed upside-down on substrate, we created a 3D environment for NPCs while still keeping their movement restricted to a unilinear condition. PDMS and substrate were coated with laminin to enhance cell adhesion. NPCs were seeded on one side of the mould and invading cells were observed to probe the tunnel first with protrusions before crawling inside the tunnel and migrating along it (Figure 5.14 a). Apparently, NPC were using the channel walls to attach and move forward (Figure 5.14 a, white circles). By employing our reporter cell line with nucleus and actin labels (chapter 4), this set-up opens the possibility to track migration in microchannels as well as observe the explorative behaviour by following the GFP-labelled actin polymerization. Statistical analysis as performed on 2D substrate and lines (sections 5.2.1 and 5.2.2), would be highly interesting yielding more insight into NPC motion

in a 3D-confined environment. However, due to technical reasons and time constraints, this data set could not be analysed.

An additional element cells regularly encounter *in vivo* are spatial confinements with sizes smaller than the cell diameter. To overcome these obstacles and squeeze through narrow pores, cell migration critically depends on cellular shape adaptation [40]. While the cytoplasm and plasma membrane are flexible, the nucleus is the largest organelle with stiffness values 2-10- fold higher than the surrounding cytoplasm [41, 42], making it the main restricting component in migration [43, 44].

By creating 3D microchannels with constrictions, we created an easy system to observe NPC dynamics and behaviour upon encountering spatial confinement with sizes smaller than their nucleus diameter. Performing a time-lapse of an imaging period of several hours with images taken every 30 sec, we captured a cell squeezing its nucleus through the restriction (Figure 5.14 b). From the start of the imaging period, where the front tip of the nucleus was already within the constriction (t = 0 min), this NPC needed 260 min to push through until the rear tip of the nucleus reached the constriction. Interestingly, squeezing the first part of the nucleus took more time and once the cell nucleus was half through the confinement (Figure 5.14 b; star) after 180 min, the pushing accelerated. From here, it took only 80 min until the second part of the nucleus was through the constriction. As overcoming this kind of confinement influences the migration time, collecting and evaluating these dynamics will be valuable to learn about the dynamics of NPCs while migrating *in vivo*.

Another interesting element observed here were the fixed attachment sides of the cytoskeleton at the channel walls (Figure 5.14 b, first image white circles). Seemingly, they were used as ankers which the cell used to push away from as well as pull towards to, and remained the same throughout the imaging time. As an example, as zoom in of the upper attachment side at the constriction shows the actin polymerization (Figure 5.14 c) and thus force generation of the cytoskeleton [45, 46].

In contrast to the fixed attachment sides, the filopodia were highly dynamic (Figure 5.14 d) and might have also served as an additional force generation or had just an explorative function. The microchannel system mimics the bigger gaps in the extracellular matrix (ECM) through which NPCs are migrating. Additionally, it approaches environment of the rostral migratory stream highway on which neuroblasts move along [47]. Additional constrictions mimic small pores of the ECM. Together, this system provides a simple approach to learn more about how NPC overcome obstacles *in vivo* and regulate their shape and nuclear dynamics.

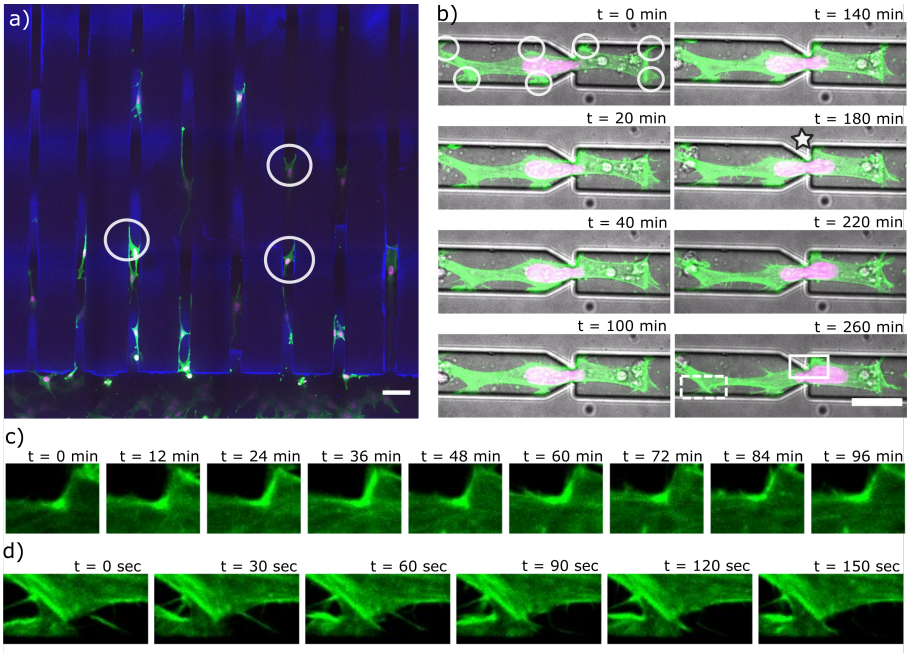

Figure 5.14: NPCs moving through microchannels and confinement. a) NPCs move along microchannels using the walls to move forward (white circles). Scale bar is 100 μm. b) Time-lapse imaging of a cell pushing its nucleus through a confinement, exhibiting stable attachment sides throughout the process (white circles). Scale bar is 50 μm. c) White rectangle from last image b. Zoom in of cell attachment side, showing on attachment side, showing actin polymerization (bright green) to generate force against the channel wall. d) White dashed rectangle from last image in b. Zoom showing that the pseudopodia are highly mobile.

CONCLUSIVE BULLET POINTS

Here the results of the current subchapter are summarized:

- Microchannels mimic bigger gaps in the extracellular matrix through which NPCs migrate *in vivo* while constrictions model small pores that NPCs need to squeeze through while migrating
- In microchannels, NPCs use channel walls to attach and move along
- When squeezing through a constriction, NPCs use fixed attachment sides to generate force for pushing away and pulling towards
- While attachment sides are fixed, filopodia are highly dynamic throughout the squeezing process

5.2.5. CONCLUSIONS

Neural progenitor cells (NPCs) have high regenerative capacity and are highly promising for therapeutic applications in neurodegenerative diseases and central nervous system injuries. Thus, understanding their innate behaviour and migratory patterns is crucial for the development of successful treatment. Minimalistic *in vitro* systems help to deconstruct the high *in vivo* complexity and provide valuable insights that contribute to this understanding. Although these systems were used to research other cell types [2], literature investigating NPC migration under standardized microenvironments *in vitro* is missing.

Here, we employed various minimalistic systems and performed statistical analysis as well as visual observations to acquire data on NPC dynamics. The focus was to establish these systems for NPC and to produce preliminary statistical output as well as qualitative assessment.

The experiments showed that NPCs move in a persistent random walk (PRW) on 2D uniform ECM substrate as well as 2D ECM-printed lines. Qualitative analysis of NPCs on patterned lines and more complex 2D geometries provided insights a set of behavioural patterns these cells express innately and as a reaction to the environment. Lastly, testing NPC dynamics in microchannels with and without constrictions, showed that the cells readily invade the channels and squeeze their nucleus through small pores while using the channel walls as support to push against and pull forward.

The generated results contribute to fundamental understanding of NPC dynamics. The calculated values of NPC speed, diffusion, and persistence time can be used for theoretical modelling to establish predictions of NPC migration under different scenarios. Further insights can be used to control NPC recruitment and tissue patterning for therapeutic applications.

After validating the minimal systems introduced here, the next step would be to combine them and thus creating a higher complexity set-up yielding more data on NPC dynamics. By creating microchannels with constrictions in a big honeycomb geometry, seeding NPCs on one side and placing a chemoattract on the other side, the *in vivo* situation can be mimicked whereby neuroblasts exit the rostral migratory stream (RMS) to move towards an injury. Adding different sizes of constrictions would give more insight into their deformation capacity and influence of small pores *in vivo* on migration speed and route choice. Alternatively, by presenting neurons and astrocytes that were damaged by high laser exposure (instead of a chemoattract), a more sophisticated system could be established providing the additional possibility to observe NPC differentiation and integration into the neural network. Once established, different types of neuroblast precursors [48] can be tested to investigate possible differences in their motility patterns.

In this chapter, for the first time (to our knowledge) neural progenitor cells were exposed to standardized microenvironments and preliminary statistical and visual data on their dynamics was collected. Expanding these experiments and learning more about the fundamental motility patterns of NPCs, as well as testing their response to various obstacles under controlled conditions, will be crucial for the establishment of successful treatments of neurodegenerative diseases and CNS injuries.

5.3. MATERIALS AND METHODS

5.3.1. PREPARATION OF PDMS STRUCTURES

To prepare the master slide, the design of the pattern was created by constructing a stereolithography CAD (computer-aided design) file (STL format). The CAD design was converted to laser coordinates using Nanowrite (Nanoscribe). The 3D structure was then exposed in a photoresist (IP-S, Nanoscribe)via two-photon polymerisation (2PP) with the Photonic Professional GT2 equipment (Nanoscribe) (these steps were performed and master mould provided by J. A. J. Wondergem). This master mould was subsequently used to prepare a patterned poly(dimethylsiloxane) (PDMS) stamps. PDMS (Sylgard 184, Dow Corning) is a two-component silicon elastomer which consists of a prepolymer and a curing agent. The prepolymer was mixed with the curing agent in a ratio of 1:10 and desiccated at 60 mbar for 1 h (MZ2NT, vacuubrand), ensuring escape of trapped air. In parallel, an adjacent vacuum chamber was used to deposit a Trichloro(1H,1H,2H,2H-perfluorooctyl)silane layer (448931, Sigma), on the master mould to ensure that PDMS can be peeled off easily later. Next, PDMS was poured over the master mould and vacuum applied again (60 mbar 1h) to ensure that the polymer enters all tunnels. Lastly, the structure was baked at 110 °C for 3h (or at 90 °C overnight) in an oven (Melag) to solidify the PDMS. After cooling down, the stamp was cut and peeled off ready for experimental use.

5.3.2. FABRICATION OF 2D PATTERNS AND MICROCHANNELS

ECM protein coating (for section 5.2.1)
A 35 mm μ-Dish (uncoated, 81151, Sigma) was open placed into a UV chamber (UVO Cleaner, Jelight Company Inc.) and exposed to UV light for 10 min. Subsequently, the dish was covered with either 1-2 μg/mL laminin (Merck, L2020) in DMEM for at least 1 h in the incubator at 37 °C or covered with fibronectin (F1141; Sigma) diluted 1:10 in MilliQ for 1 h at room temperature.

μCP of Fibronectin lines (for section 5.2.2)
To produce 2D line pattern micro-contact printing (μCP) technique was used. The PDMS pattern was exposed for 15 min to UV (UVO Cleaner, Jelight Company Inc.) and then a drop of fibronectin solution was deposited on its surface and incubated for 30 min in the dark. Fibronectin solution: 50 μg/ml fluorescent fibronectin linked with Alexa Fluor 647 (kindly provided by Schmidt group) was mixed with 10 μg/ml un-labelled fibronectin and filled to 40 μl with MilliQ water. After incubation, not adsorbed fibronectin was washed away with MilliQ and left for 20 min to dry in the cell culture hood. An uncoated 35 mm μ-Dish (81151, ibidi) was exposed to UV light for 15 min to activate its surface. The PDMS stamp was flipped onto the dish surface, gently pressed down, and incubated for 30 min in the dark. Subsequently, the stamp was removed, and the dish was washed with 70% ethanol and covered with 0.25% Pluronic F-127 for 1h. Finally, the dish was washed 2x with PBS and used for cell seeding and experiments. Alternatively, the patterned dish could be stored for maximum 2 days at 4 °C before use.

μPIP of honeycomb and square patterns (for section 5.2.3)
For the microscale plasma-induced patterning (μPIP), the PDMS pattern was cut along the pattern borders to ensure that plasma can flow in every tunnel. The cut PDMS was placed onto an uncoated 35 mm μ-Dish (81151, ibidi) with the pattern facing downwards and gently pressed down. Next, the dish with the PDMS was exposed to plasma for 6 min (Plasma-Surface-Technology, Diener electronic). When finished, the stamp was gently removed, and the surface covered with 0.2% Pluronic F-127 for 1h at room temperature. To return to sterile conditions, the dish was washed with 70% Ethanol and 2x with PBS. The dish was covered with a laminin solution (1-2 μg/ml) and incubated for 1h in the incubator at 37 °C. Finally, the patterned dish could be used for experiment or be stored for maximum 1 day in the incubator at 37 °C before use.

Microchannels and constrictions (for section 5.2.4)
To ensure cell invasion, the PDMS pattern had to be cut along the start of the channels. For microchannels, an ibiTreat 35 mm μ-Dish (81156, ibidi) was used. The PDMS pattern was exposed for 15 min to UV light (UVO Cleaner, Jelight Company Inc.) and incubated with fibronectin solution as described in section above to ensure cell attachment and visualize the lines. For microchannels with confinement, an ibiTreat 4 Well μ-Slide was used (80426, ibidi) and the PDMS pattern was exposed 15 min to UV (UVO Cleaner, Jelight Company Inc.) and incubated with 1:10 fibronectin (F1141, Sigma) solution in MilliQ. In both cases, the PDMS pattern was flipped onto the dish surface, gently pressed down and the dish was covered with cell culture media. Then, the dish was placed without the lid into a p60 culture dish, and its lid closed and exposed to vacuum for 10 min at 20 mbar (MZ2NT, vacuubrand) to facilitate fluid perfusion throughout the channels. Lastly, the structure was used for experiments or was stored for maximum 1 day in the incubator at 37 °C before use.

5.3.3. CELL CULTURE

C17.2 cells (Merck, 07062902) were cultured as described in chapter 4. NPCs with labelled actin and nuclei were generated via transduction as described in chapter 4.

5.3.4. LIVE CELL IMAGING

Cells were imaged with a Nikon Eclipse Ti-E inverted microscope (Nikon Instruments Europe, Netherlands), equipped with a spinning disk unit (Yokogawa, 10,000 rpm). An automated XY stage facilitated imaging multiple fields of view. Positions were illuminated either with 488 nm, 561 nm, and/or 647 nm lasers (Agilent MLC400 monolithic laser combiner, Agilent Technologies, Netherlands), and/or with bright-field. Images were captured with an Andor iXon Ultra 897 High-speed EM-CCD camera. Image acquisition was automated using NisElements software (LIM, Czech Republic). Stable conditions throughout the measurements were ensured by using a Tokai Hit stage incubator set to 37 ∘C and 5% CO2. The incubator is equipped with a water bath to maintain a certain humidity.

Imaging specifics. Section 5.2.1: Plan Apo λ 20x objective, large image 6x6, time-lapse with imaging period of 20 h and images taken every 10 min with 488 nm and 561 nm lasers to visualize the actin network and cell nuclei, respectively. Section 5.2.2: Plan

Apo λ 20x objective, large image 6x10, time-lapse with imaging period of 22h and images taken every 10 min with 488 nm and 561 nm lasers to visualize the actin network and cell nuclei, respectively. At the end of the experiment, one image with 647 nm illumination was performed to visualize the patterned lines. Section 5.2.3: Plan Fluor 10x Ph1 DLL, multiple positions 30 XY, time-lapse with imaging period of 15 h and images taken every 1 min with brightfield. Section 5.2.4 5.1.4: a) microchannels: Plan Apo λ 20x objective, large image 12x6, time-lapse with imaging period of 48 h and images taken every 15 min with 488 nm, 561nm, and 647 nm to visualize actin, cell nuclei, and fibronectin-labelled lines. b) microchannels with confinement: Plan Apo λ 60x Oil objective, time-lapse with imaging period of 35 min and images taken every 30 sec with 488 nm and 561 nm lasers to visualize the actin network and cell nuclei, respectively, and brightfield to visualize the channel.

5.3.5. CELL TRACKING AND ANALYSIS

Cell movement was analysed by tracking the nucleus of the cells. Fluorescent time-lapse images (excitation at 561 nm) were rendered into binary images using ImageJ (http://imagej.nih.gov/ij/). Tracking was performed using the Image J Plugin TrackMate [49], whereby all trajectories had to be corrected manually. With each cell division, a new trajectory was started and trajectory lengths with less than 30 points were omitted. Based on this data, trajectory length and directions, and movement statistics based on the mean squared displacement (MSD) were calculated and plotted, using a home-made Matlab algorithm written by J. A. J. Wondergem. The MSD measures the space a cell explores over time. The trajectory data are arrays of the position r(t) = x(t) + y(t) of the cell at time t. The displacement δ r is given by

$$\delta r(t) = r(t+\delta t) - r(t) \tag{5.1}$$

where δt is the inverse frame rate. The MSD of a cell trajectory is defined as the average of squared displacements for all lag times τ = k δ t, given by

$$\langle \delta r(\tau)^2 \rangle = \frac{1}{N-k} \sum_{i=1}^{N-k} (r(t_i+\tau) - r(t_i))^2 \tag{5.2}$$

where N is the number of points in the trajectory and k = 1, 2,..., N - 1.

ll values of the MSD are averaged over the number of trajectories. The 95% confidence bounds were determined by using a t-distribution using an α value of 2.5% and the degrees of freedom set to the number of trajectories.

To analyse the trajectory data, we used an MSD PRW fit (equation 1.1) and an MSD linear fit to diffusive regime (equation 1.3). Specifically, the MSD curve was fitted to the following formula derived for a 2D PRW [50]:

$$\langle \delta r(\tau)^2 \rangle = 2v^2\tau_p^2\left(\frac{\tau}{\tau_p} + e^{\frac{-\tau}{\tau_p}} - 1\right) \tag{5.3}$$

where τ is the lag time, v is the instantaneous velocity, and τ_p the persistence time. Fitting the MSD to this equation allows to extract the migration parameters v and τ_p. For fits of 1D motion, the factor of 2 drops out of equation 1.3.

At short timescales ($t << \tau_p$), the motion described by equation 4.3 is ballistic ($\langle \delta r(\tau)^2 \rangle \approx (vt)^2$) due to persistence in orientation of the cell. At long timescales ($t >> \tau_p$), equation 4.3 is approximated by $\langle \delta r(\tau)^2 \rangle \approx 2v^2 2\tau_p t$ (for fits in 1D, this becomes $\approx v^2\tau_p$ t), which describes diffusive motion.

To find an effective diffusion coefficient D_eff, the MSD was fitted linearly at long times using the formula:

$$\langle \delta r(\tau)^2 \rangle \xrightarrow{\tau \gg \tau} 4D_eff\tau \tag{5.4}$$

For fits of 1D motion, the factor of 4 becomes 2 in equation 1.4. Subsequently, the average velocity (v) was extracted based on the calculated velocities using $\delta r/\delta$ t.

5.4. REFERENCES

[1] Ramsés Ayala, Tianzhi Shu, and Li-Huei Tsai. "Trekking across the brain: the journey of neuronal migration". In: *Cell* 128.1 (2007), pp. 29–43.

[2] Juan Manuel Garcia-Arcos et al. "Reconstitution of cell migration at a glance". In: *Journal of cell science* 132.4 (2019), jcs225565.

[3] Antonetta BC Buskermolen et al. "Entropic forces drive cellular contact guidance". In: *Biophysical journal* 116.10 (2019), pp. 1994–2008.

[4] Amélie Béduer et al. "Engineering of adult human neural stem cells differentiation through surface micropatterning". In: *Biomaterials* 33.2 (2012), pp. 504–514.

[5] Arjan P Quist and Sven Oscarsson. "Micropatterned surfaces: techniques and applications in cell biology". In: *Expert opinion on drug discovery* 5.6 (2010), pp. 569–581.

[6] Menekse Ermis, Ezgi Antmen, and Vasif Hasirci. "Micro and Nanofabrication methods to control cell-substrate interactions and cell behavior: A review from the tissue engineering perspective". In: *Bioactive materials* 3.3 (2018), pp. 355–369.

[7] Changjiang You and Jacob Piehler. "Functional protein micropatterning for drug design and discovery". In: *Expert opinion on drug discovery* 11.1 (2016), pp. 105–119.

[8] András Perl, David N Reinhoudt, and Jurriaan Huskens. "Microcontact printing: limitations and achievements". In: *Advanced Materials* 21.22 (2009), pp. 2257–2268.

[9] Bryan A Langowski and Kathryn E Uhrich. "Microscale plasma-initiated patterning (μpip)". In: *Langmuir* 21.23 (2005), pp. 10509–10514.

[10] David Selmeczi et al. "Cell motility as random motion: A review". In: *The European Physical Journal Special Topics* 157.1 (2008), pp. 1–15.

[11] Daniel Campos, Vicenç Méndez, and Isaac Llopis. "Persistent random motion: Uncovering cell migration dynamics". In: *Journal of theoretical biology* 267.4 (2010), pp. 526–534.

[12] Mitchell H Gail and Charles W Boone. "The locomotion of mouse fibroblasts in tissue culture". In: *Biophysical journal* 10.10 (1970), pp. 980–993.

[13] Takuro Kojima et al. "Subventricular zone-derived neural progenitor cells migrate along a blood vessel scaffold toward the post-stroke striatum". In: *Stem cells* 28.3 (2010), pp. 545–554.

[14] Naoko Kaneko, Masato Sawada, and Kazunobu Sawamoto. "Mechanisms of neuronal migration in the adult brain". In: *Journal of neurochemistry* 141.6 (2017), pp. 835–847.

[15] Valerie A Liu, William E Jastromb, and Sangeeta N Bhatia. "Engineering protein and cell adhesivity using PEO-terminated triblock polymers". In: *Journal of biomedical materials research* 60.1 (2002), pp. 126–134.

[16] Kenneth R Chien, Ibrahim J Domian, and Kevin Kit Parker. “Cardiogenesis and the complex biology of regenerative cardiovascular medicine”. In: *Science* 322.5907 (2008), pp. 1494–1497.

[17] Hug Aubin et al. “Directed 3D cell alignment and elongation in microengineered hydrogels”. In: *Biomaterials* 31.27 (2010), pp. 6941–6951.

[18] Arja Ray et al. “Anisotropic forces from spatially constrained focal adhesions mediate contact guidance directed cell migration”. In: *Nature communications* 8.1 (2017), pp. 1–17.

[19] Claire Leclech and Catherine Villard. “Cellular and subcellular contact guidance on microfabricated substrates”. In: *Frontiers in Bioengineering and Biotechnology* 8 (2020), p. 1198.

[20] Paolo Maiuri et al. “The first world cell race”. In: *Current Biology* 22.17 (2012), R673–R675.

[21] Camila Londono et al. “Nonautonomous contact guidance signaling during collective cell migration”. In: *Proceedings of the National Academy of Sciences* 111.5 (2014), pp. 1807–1812.

[22] Revathi Ananthakrishnan and Allen Ehrlicher. “The forces behind cell movement”. In: *International journal of biological sciences* 3.5 (2007), p. 303.

[23] Akiyoshi Kakita and James E Goldman. “Patterns and dynamics of SVZ cell migration in the postnatal forebrain: monitoring living progenitors in slice preparations”. In: *Neuron* 23.3 (1999), pp. 461–472.

[24] Noelia Martinez-Molina et al. “Rostral migratory stream neuroblasts turn and change directions in stereotypic patterns”. In: *Cell adhesion & migration* 5.1 (2011), pp. 83–95.

[25] Michael P Sheetz et al. “Cell migration as a five-step cycle.” In: *Biochemical Society Symposium*. Vol. 65. 1999, pp. 233–243.

[26] Sang Chae Nam et al. “Dynamic features of postnatal subventricular zone cell motility: A two-photon time-lapse study”. In: *Journal of Comparative Neurology* 505.2 (2007), pp. 190–208.

[27] Rui L Zhang et al. “Patterns and dynamics of subventricular zone neuroblast migration in the ischemic striatum of the adult mouse”. In: *Journal of Cerebral Blood Flow & Metabolism* 29.7 (2009), pp. 1240–1250.

[28] Bodo Borm et al. “Membrane ruffles in cell migration: indicators of inefficient lamellipodia adhesion and compartments of actin filament reorganization”. In: *Experimental cell research* 302.1 (2005), pp. 83–95.

[29] Qing Zhang. “The Research Advance of Cell Bridges in vitro”. In: *Frontiers in Bioengineering and Biotechnology* 8 (2020), p. 1349.

[30] Antonetta BC Buskermolen et al. “Cellular contact guidance emerges from gap avoidance”. In: *Cell Reports Physical Science* 1.5 (2020), p. 100055.

[31] Manuel Théry et al. “The extracellular matrix guides the orientation of the cell division axis”. In: *Nature cell biology* 7.10 (2005), pp. 947–953.

[32] Alexandra Fink et al. “Area and geometry dependence of cell migration in asymmetric two-state micropatterns”. In: *Biophysical journal* 118.3 (2020), pp. 552–564.

[33] Christina L Dix et al. “The role of mitotic cell-substrate adhesion re-modeling in animal cell division”. In: *Developmental cell* 45.1 (2018), pp. 132–145.

[34] John R Davis et al. “Inter-cellular forces orchestrate contact inhibition of locomotion”. In: *Cell* 161.2 (2015), pp. 361–373.

[35] David Li and Yu-li Wang. “Coordination of cell migration mediated by site-dependent cell–cell contact”. In: *Proceedings of the National Academy of Sciences* 115.42 (2018), pp. 10678–10683.

[36] Elena Scarpa et al. “A novel method to study contact inhibition of locomotion using micropatterned substrates”. In: *Biology open* 2.9 (2013), pp. 901–906.

[37] Brian Stramer and Roberto Mayor. “Mechanisms and in vivo functions of contact inhibition of locomotion”. In: *Nature reviews Molecular cell biology* 18.1 (2017), pp. 43–55.

[38] Joe Steinman et al. “3D morphological analysis of the mouse cerebral vasculature: Comparison of in vivo and ex vivo methods”. In: *PloS one* 12.10 (2017), e0186676.

[39] Manuel Théry. “Micropatterning as a tool to decipher cell morphogenesis and functions”. In: *Journal of cell science* 123.24 (2010), pp. 4201–4213.

[40] Marina Krause et al. “Cell migration through three-dimensional confining pores: speed accelerations by deformation and recoil of the nucleus”. In: *Philosophical Transactions of the Royal Society B* 374.1779 (2019), p. 20180225.

[41] Haijiao Liu et al. “In situ mechanical characterization of the cell nucleus by atomic force microscopy”. In: *ACS nano* 8.4 (2014), pp. 3821–3828.

[42] Jan Lammerding. “Mechanics of the nucleus”. In: *Comprehensive physiology* 1.2 (2011), p. 783.

[43] Alexandra Lynn McGregor, Chieh-Ren Hsia, and Jan Lammerding. “Squish and squeeze—the nucleus as a physical barrier during migration in confined environments”. In: *Current opinion in cell biology* 40 (2016), pp. 32–40.

[44] Francisco J Calero-Cuenca, Cátia S Janota, and Edgar R Gomes. “Dealing with the nucleus during cell migration”. In: *Current opinion in cell biology* 50 (2018), pp. 35–41.

[45] Alex Mogilner. “On the edge: modeling protrusion”. In: *Current opinion in cell biology* 18.1 (2006), pp. 32–39.

[46] Matthew J Footer et al. “Direct measurement of force generation by actin filament polymerization using an optical trap”. In: *Proceedings of the National Academy of Sciences* 104.7 (2007), pp. 2181–2186.

[47] Archana Gengatharan, Rodrigo R Bammann, and Armen Saghatelyan. “The role of astrocytes in the generation, migration, and integration of new neurons in the adult olfactory bulb”. In: *Frontiers in neuroscience* 10 (2016), p. 149.

[48] Verónica Martínez-Cerdeño and Stephen C Noctor. “Neural progenitor cell terminology”. In: *Frontiers in neuroanatomy* 12 (2018), p. 104.

[49] Jean-Yves Tinevez et al. “TrackMate: An open and extensible platform for single-particle tracking”. In: *Methods* 115 (2017), pp. 80–90.

[50] Reinhold Fürth. “Die brownsche bewegung bei berücksichtigung einer persistenz der bewegungsrichtung. mit anwendungen auf die bewegung lebender infusorien”. In: *Zeitschrift für Physik* 2.3 (1920), pp. 244–256.